Highly Active and Stable Hydrogen Evolution Electrocatalysts Based on Molybdenum Compounds on Carbon Nanotube–Graphene Hybrid Support

Duck Hyun Youn,[†,⊥] Suenghoon Han,[‡,⊥] Jae Young Kim,[†] Jae Yul Kim,[†] Hunmin Park,[‡] Sun Hee Choi,[§] and Jae Sung Lee[†,*]

[†]School of Energy and Chemical Engineering, Ulsan National Institute of Science and Technology (UNIST), Ulsan 689-798, Korea, [‡]Department of Chemical Engineering, Pohang University of Science and Technology (POSTECH), Pohang 790-784, Korea, and [§]Pohang Accelerator Laboratory (PAL), Pohang University of Science and Technology (POSTECH), Pohang 790-784, Korea. [⊥]D. H. Youn and S. Han contributed equally.

ABSTRACT Highly active and stable electrocatalysts for hydrogen evolution have been developed on the basis of molybdenum compounds (Mo_2C, Mo_2N, and MoS_2) on carbon nanotube (CNT)–graphene hybrid support *via* a modified urea-glass route. By a simple modification of synthetic variables, the final phases are easily controlled from carbide, nitride to sulfide with homogeneous dispersion of nanocrystals on the CNT–graphene support. Among the prepared catalysts, Mo_2C/CNT–graphene shows the highest activity for hydrogen evolution reaction with a small onset overpotential of 62 mV and Tafel slope of 58 mV/dec as well as an excellent stability in acid media. Such enhanced catalytic activity may originate from its low hydrogen binding energy and high conductivity. Moreover, the CNT–graphene hybrid support plays crucial roles to enhance the activity of molybdenum compounds by alleviating aggregation of the nanocrystals, providing a large area to contact with electrolyte, and facilitating the electron transfer.

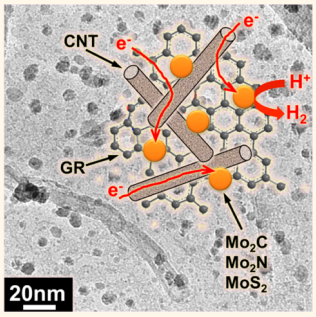

KEYWORDS: hydrogen evolution reaction · nonprecious metal electrocatalysts · molybdenum carbide · molybdenum nitride · CNT–graphene hybrid

Hydrogen is projected as a promising energy carrier of the future replacing fossil fuels because it is CO_2-neutral and of high gravimetric energy density.[1,2] To take a full advantage of the desirable characteristics of hydrogen, it should be produced from a renewable energy source in a sustainable manner. Recently, much attention has been paid to generation of hydrogen from electrochemical or photoelectrochemical water splitting powered by renewable energy sources including wind or solar energies.[3] Hydrogen evolution reaction (HER) is a key step in water splitting, whereby protons and electrons are combined into molecular hydrogen. At present, platinum is the most efficient and typical electrocatalyst for HER in acid media,[4,5] but its high cost and scarcity have hampered the large-scale hydrogen production through acidic electrolyzers like polymer electrolyte membrane (PEM) electrolyzers. The same electrocatalyst is also in demand as a cathode of photoelectrochemical water splitting cells. Thus, the development of efficient electrocatalysts for HER with earth-abundant materials is the crucial challenge for practical large-scale hydrogen production.

Transition metal carbides, nitrides, and sulfides are known as effective candidates for replacing the Pt group metals in various catalytic processes including hydrogenation and hydrodesulfurization due to their similar electronic structures to that of noble metals.[6,7] These materials have attracted a wide range of interest in energy applications encompassing fuel cells,[8,9] photocatalysts,[10,11] solar cells,[12,13] and HER.[14,15] Particularly in HER field, Mo-based chalcogenides have been investigated extensively.[16–20] Molybdenum carbides and nitrides have received much less attention just as a support material for noble metals to enhance its activity.[3] Only recently, they are also recognized as efficient catalysts for HER without noble metals.[14,15,21–23] Vrubel *et al.* reported

* Address correspondence to jlee1234@unist.ac.kr.

Received for review March 1, 2014 and accepted April 30, 2014.

Published online April 30, 2014
10.1021/nn5012144

the activity of Mo_2C and MoB in both of acid and base media.[14] Carbon-supported nickel molybdenum nitride exhibited excellent activity with a very small Tafel slope value of 35 mV dec^{-1}.[15] Chen *et al.* synthesized Mo_2C/CNT composite by calcination under Ar flow, which exhibited good onset overpotential and high current density.[21] Same group fabricated Mo_2N–Mo_2C composite (named Mo_1Soy) using soybean as carbon and nitrogen sources. The Mo_1Soy presented remarkably high HER activity with increased durability.[22] Liao *et al.* prepared nanoporous Mo_2C nanowires by pyrolysis of a MoOx/amine precursor under an inert atmosphere.[23] Their catalyst showed low onset overpotential and high mass activity. Hence at this point, there is a need to establish the HER activity of Mo-compounds, *i.e.*, the molybdenum carbide, nitride, and sulfide, among themselves and relative to the conventional Pt catalyst.

Herein, we report a general synthetic method encompassing Mo_2C, Mo_2N, and MoS_2 with carbon nanotube (CNT)–graphene (GR) composite by a modified urea-glass route developed by our research group.[8,13] Our synthetic procedure is highly phase selective, *i.e.*, a pure form of nanocrystalline Mo_2C, Mo_2N, or MoS_2 is easily fabricated on a CNT–GR hybrid support by simply varying the amount of urea or using thiourea instead of urea. The CNT–GR hybrid support (an optimized 1:1 composite between CNT and GR) was introduced to enhance the HER activity of the loaded Mo-compounds by multiple ways: (i) to stabilize Mo-compound nanoparticles, (ii) to provide a large surface area for facile contact with electrolyte, and (iii) to provide an excellent electron pathway to and from catalyst particles. To the best of our knowledge, this is the first systematic study to reveal the relative activity of Mo-compounds for HER on a fair ground by developing a general synthetic method to produce these Mo compounds under the same conditions except the amount of urea (or thiourea) to control the phase of the product. In addition, the effectiveness of CNT–GR hybrid is demonstrated as a highly efficient electron transfer medium that brings the best HER activity of these Mo compounds.

Our results are significant in several aspects: First, Mo_2C, Mo_2N, and MoS_2 on CNT–GR hybrid were prepared by an identical and simple synthetic method in solution phase. By varying the amount of urea or replacing urea with thiourea, we could control the final phase precisely. During the synthetic procedure, no toxic reactant gases such as CH_4, NH_3, and H_2S were used. Furthermore, additional reduction step was not required because of simultaneous reduction of GO to GR by thermal annealing during the synthetic procedure. Second, the activity comparisons among Mo_2C, Mo_2N, and MoS_2 on CNT–GR composites were properly carried out on the common ground by adopting a general synthetic method for all materials. In general,

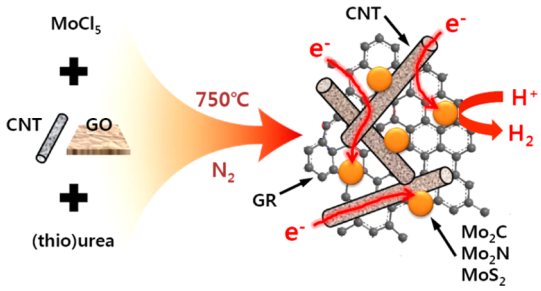

Scheme 1. Schematic illustration of our synthetic method and resultant Mo-compounds on CNT–GR hybrid support for hydrogen evolution.

fabrication methods affect the properties and activities of catalysts greatly. Therefore, preparation of the catalysts by one general method is imperative for proper activity comparison by removing the variables originating from the synthetic method. Third, our non-precious metal catalyst, Mo_2C/CNT–GR exhibited very high activity and durability for HER, recording one of the best performances among Mo-based catalysts reported so far. We believe that the present work could be a guideline in selecting a viable non-noble metal catalyst for HER and enhancing the activity of the catalyst by adopting a proper hybrid of low dimensional carbon allotropes.

RESULTS AND DISCUSSION

Physicochemical Properties of the Prepared Electrocatalysts. Scheme 1 illustrates our synthetic method and a schematic model of a Mo-compound loaded on CNT–GR composite. In ethanol solution containing CNT and graphene oxide (GO), the metal precursor $MoCl_5$ reacted vigorously with ethanol to form Mo orthoester. Addition of urea in a urea/metal molar ratio (R) of 1 to the solution yielded a metal-urea complex on CNT–GO. Upon heat treatment under N_2 atmosphere at 750 °C, Mo_2N/CNT–GR was obtained. When R value was increased to 8, Mo_2C/CNT–GR was generated instead of Mo_2N. The nitrogen and oxygen were removed from the precursor as NO_x during the heat treatment.[24] Thus, the remaining carbon atoms were bonded to Mo to produce Mo_2C/CNT–GR. The replacement of urea with thiourea (R = 2) allowed the fabrication of MoS_2/CNT–GR. Notably, GO in the CNT–GO composite is reduced to GR by thermal annealing[25] simultaneously with the formation of Mo_2C, Mo_2N, and MoS_2 nanocrystals on the support, and thus no additional loading or reduction process are required.

The CNT–GR hybrid support plays important roles in forming active HER catalysts. First, it provides a large surface area needed for the loaded Mo-compounds to contact readily with the liquid electrolyte. When used singly, CNTs and GR layers tend to be bundled or stacked with each other to reduce the surface energy. This general behavior of one- and two-dimensional

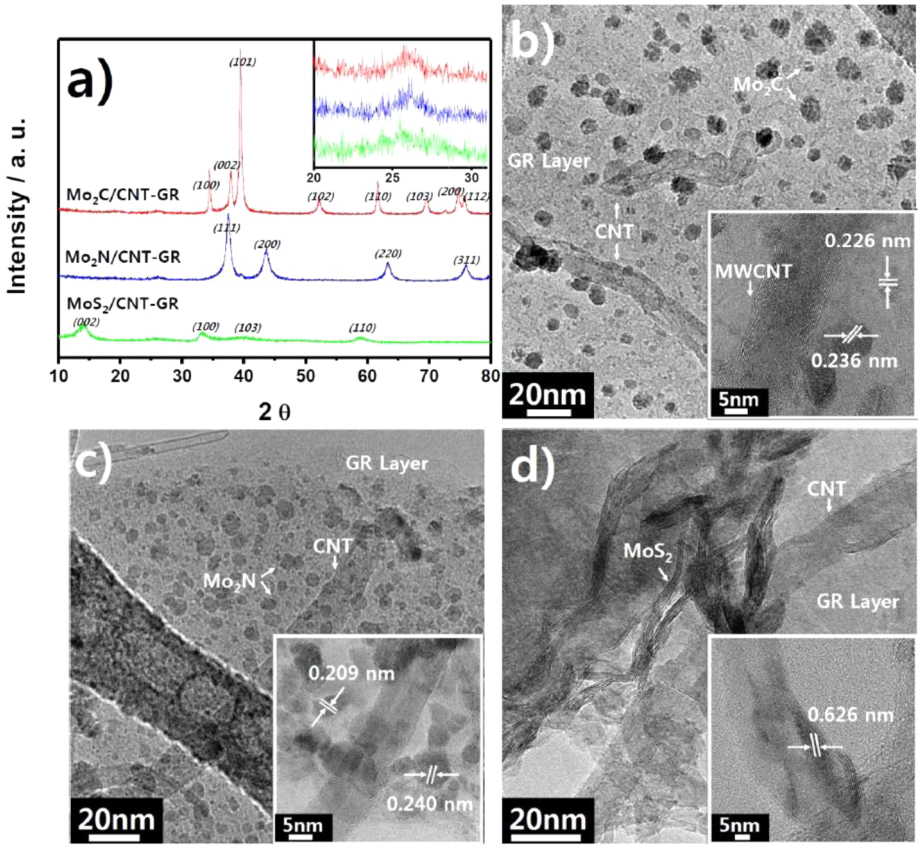

Figure 1. (a) XRD patterns of the synthesized catalysts. The inset in (a) denotes the magnified patterns in the range of 20−30°. TEM images and the corresponding high-resolution TEM images of (b) Mo_2C/CNT−GR, (c) Mo_2N/CNT−GR, and (d) MoS_2/CNT−GR. Enlarged inset images of (b−d) are presented in Figure S1 (SI).

carbon allotropes reduces the surface area and deteriorates the conducting property. By acting as a spacer for each other, the CNT−GR composite could alleviate the bundling (CNT) and stacking (GR) problems by forming a three-dimensional heterostructure. Second, it provides an excellent electron conducting pathway to the Mo-compounds. By providing a large surface area and high conductivity to Mo-compounds, the CNT−GR composite could substantially increase the number of active sites (contact area between metal and electrolyte) and the unit activity of each site (by enhanced electron transfer), and thus offers the enhanced activity of Mo-compounds for HER.

The XRD patterns of the Mo_2C, Mo_2N, and MoS_2 supported on the CNT−GR hybrid are shown in Figure 1a, which are consistent with their reference XRD patterns of hexagonal Mo_2C (JCPDS No. 00−035−0787), cubic Mo_2N (00−025−1366) and hexagonal MoS_2 (01−075−1539). No peaks of byproducts (Mo metal or MoO_x) were observed indicating effectiveness of our synthetic method to fabricate the pure phase of Mo_2C, Mo_2N, and MoS_2 on CNT−GR hybrid support. By Scherrer equation, the mean particle sizes of Mo_2C and Mo_2N were estimated to be 9.5 and 7.6 nm, respectively. The MoS_2 catalysts showed layered structure demonstrated by (002) peak at 14° attributed to the stacked layers of MoS_2. A small peak observed at 24−26° was originated from the CNT−GR support (inset of Figure 1a),[26] and absence of peaks around 10° confirmed that GO was effectively reduced to GR by thermal annealing.[25] The formation of GR was further verified by Raman spectra as discussed later.

Structural details of the prepared catalysts were analyzed by high-resolution TEM in Figure 1b−d and Figure S1 (Supporting Information (SI)). In all cases, CNTs were distributed randomly on GR layers. In the TEM images of Mo_2C/CNT−GR (Figure 1b) and Mo_2N/CNT−GR (Figure 1c), spherical particles of Mo-compounds were dispersed well over the CNT−GR hybrid support without free-standing particles located away from the support. In stark contrast, bare Mo_2C and Mo_2N without CNT−GR support showed serious aggregation of the particles producing large clusters above several micrometer size (Figure S2 (SI)). This represents another beneficial role of CNT−GR hybrid support in dispersing Mo-compound nanoparticles without the serious aggregation. These observations are common in bare and supported MoS_2 catalysts, which provide evidence for a good coupling effect between Mo-compounds and CNT−GR support. The mean particle sizes of Mo_2C and Mo_2N collected from TEM images are 9.6 and 8.0 nm, which are consistent

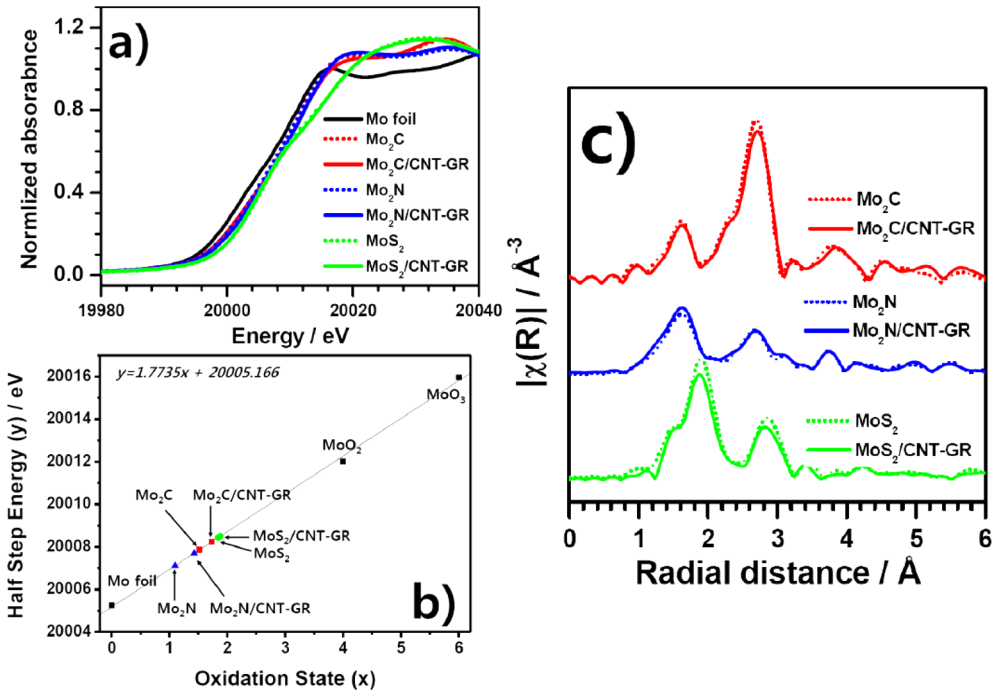

Figure 2. (a) Mo K-edge XANES spectra of bare and supported catalysts, (b) correlation between the half step energy of the Mo K-edge with the oxidation state of various Mo-compounds, (c) Fourier-transforms of Mo K-edge EXAFS for the bare and supported catalysts.

with the results estimated from the XRD patterns. In inset of Figure 1b, lattice spacing values of 0.236 and 0.226 nm were observed corresponding to the *d*(002) and *d*(101) of Mo_2C. The lattice fringes of 0.240 and 0.209 nm shown in inset of Figure 1c are well-matched to the *d*(111) and *d*(200) of Mo_2N, respectively. In contrast, MoS_2 displayed a layered structure consisting of 4−10 layers on CNT−GR support. The distance between the layers was 0.626 nm corresponding to *d*(002) of MoS_2. Layered MoS_2 nanocrystals are somewhat aggregated rather than dispersed homogeneously on the CNT−GR support compared to the previously reported nanocarbon-supported MoS_2 prepared at lower temperatures[17,27,28] and our synthesized Mo_2C/CNT−GR and Mo_2N/CNT−GR catalysts.

The electronic and local structures of Mo in the synthesized catalysts were examined by X-ray absorption fine structure (XAFS). In Figure 2a, the X-ray absorption near edge structure (XANES) spectra of Mo K-edge for the supported Mo-compounds are compared with Mo foil and unsupported Mo-compounds. The absorption edges of bare and supported catalysts, denoting an electric dipole transition from Mo 1s core level to unoccupied states of p type, were shifted to higher energies compared to the Mo foil. The correlation between Mo K-edge half-step energy and oxidation state was examined in Figure 2b. The half-step energy of Mo foil of zero oxidation state was measured to be 20005.2 eV as reported.[21] Notably, the half-step energies of both bare and supported compound catalysts were higher by *ca.* 2−3 eV compared to Mo foil. This reflects the prevalent ionic character Mo in the compounds over metallic or covalent character due to the significant charge transfer from metal to nonmetal atom.[7] Hence, Mo in the compounds is not fully oxidized but in a significantly electron deficient state ($Mo^{\delta+}$) with the extent increasing in the sequence of Mo_2N < Mo_2C < MoS_2. As noted by Liu *et al.*, the more positively charged Mo atoms indicate the lowered d-band center.[29] The down-shifted d-band center of Mo atoms in the compounds could reduce the hydrogen binding energy and thus greatly affect the HER activity.[21] Considering Mo metal generates a strong metal−hydrogen bonding, the lowered hydrogen binding energy is a desirable change for HER. Thus, Mo atoms in Mo_2C possess more positive charge than those of Mo_2N, and the hydrogen binding energy of Mo_2C would be lower, and thus its HER activity is higher compared to Mo_2N. When the Mo-compounds are loaded on CNT−GR support, the half-step energy increased suggesting the charge transfer from metal to support. The differences between bare and supported catalysts are relatively small compared to those between Mo-compounds, because charges of Mo atoms are already effectively transferred to nonmetal atoms of C, N, and S. But the same trend in the extent of the charge transfer is maintained in both unsupported and supported Mo compounds.

Figure 2c displays the Fourier-transformed extended X-ray absorption fine structure (EXAFS) spectra of the Mo composite catalysts with their fitting parameters summarized in Table 1. Bare and supported

catalysts in each phase possess almost the same local structures around a central Mo atom. A particular attention should be paid that no oxide-related peaks are observed in the EXAFS spectra of supported catalysts. It suggests that oxide species generally formed on the surface of Mo_2C and Mo_2N[30,31] hardly affects the local structure of these catalysts. However, in sulfide, the surface oxide species is identified as MoO_3 in both normalized spectra and their derivatives of Mo K-edge XANES (Figure S2 (SI)). Thus, the higher half-step energies of MoS_2 catalysts in Figure 2b could be partly derived from the formation of surface oxide species. As MoO_3 is known as inactive for HER, the surface oxide formation should have lowered HER activity of MoS_2/CNT−GR more than Mo_2C/CNT−GR and Mo_2N/CNT−GR.

To confirm that the different electronic states of Mo-compounds is indeed reflected on their hydrogen binding energy, which is a good descriptor for HER activity,[21] hydrogen temperature-programmed desorption (H_2-TPD) measurements were conducted. In Figure S4 (SI), H_2 desorption temperature of Mo_2C/CNT−GR was in the range of 150−350 °C with a peak at 220 °C. Mo_2N/CNT−GR exhibited a broader H_2 desorption temperature window (150−370 °C) and a higher peak temperature (245 °C). Thus, hydrogen binding energy of Mo_2C/CNT−GR is weaker than that of Mo_2N/CNT−GR, which is consistent with the XANES analysis. In case of MoS_2/CNT−GR, a relatively broad desorption temperature window was observed from 160 to 450 °C with multiple H_2 desorption peak temperatures. Higher H_2 desorption temperature of MoS_2 than those of Mo_2C and Mo_2N was also observed in the previous works.[6,32−35] Thus, the H_2-TPD results generally support the XANES analysis and the lower hydrogen binding energy of Mo_2C/CNT−GR than those of Mo_2N/CNT−GR, and MoS_2/CNT−GR could be responsible for their highest HER activity.

Conductivities of the synthesized catalysts were measured by the four point probe method, and the results are summarized in Table 2. In general, because of the aid of conducting CNT−GR support, the supported catalysts exhibit a good conductivity, order of $\sim 10^3$ S m^{-1}, except for MoS_2/CNT−GR showing 1.06×10^2 S m^{-1}. As shown in TEM images, MoS_2 nanocrystals on CNT−GR are fairly aggregated compared to Mo_2C or Mo_2N nanocrystals. Thus, electrically less conductive MoS_2 crystals might hinder the electron transfer in the catalyst. Mo_2C/CNT−GR exhibits the best conductivity of 3.10×10^3 S m^{-1}, which is 1.7 and 30 times higher value than those of Mo_2N/CNT−GR and MoS_2/CNT−GR, respectively. A good conductivity is an essential requirement to be an efficient electrocatalyst, which was easily achieved here by dispersing Mo-compounds on CNT−GR.

HER Activities and Electrochemical Properties. Figure 3a displays the polarization curves for HER of the synthesized catalysts with commercial Pt/C (20 wt %, E-TEK) catalysts. As well-known, Pt/C exhibited a high activity for HER with nearly zero onset overpotential (η) and high current density. Among the synthesized catalysts, Mo_2C/CNT−GR showed the smallest η of 62 mV compared to Mo_2N/CNT−GR (118 mV) and MoS_2/CNT−GR (140 mV). In addition, the current density of Mo_2C/CNT−GR was higher than the other electrocatalysts in the whole potential region. Such a low η and high current density of Mo_2C/CNT−GR demonstrates the high activity of Mo_2C sites as well as the large number of Mo_2C sites.

For further investigation of HER activity, Tafel plots were fitted to Tafel equation ($\eta = a + b \log|J|$), where J is the current density and b is the Tafel slope. In Figure 3b, commercial Pt showed the Tafel slope of 30 mV/dec, which is corresponding to the reported values confirming the validity of our electrochemical measurements. The Tafel slope of Mo_2C/CNT−GR was 58 mV/dec, which outperformed the Mo_2N/CNT−GR (72 mV/dec) and MoS_2/CNT−GR (100 mV/dec), respectively. Notably, bare Mo-compounds without CNT−GR support exhibited very low HER performances and resultant high Tafel slopes, although their activity trend was the same as that of the supported Mo-compounds (Figure S3 (SI)). These results demonstrate dramatic effects of CNT−GR hybrid in enhancing the activity of

TABLE 1. Structural Parameters Calculated from Mo K-edge EXAFS Fits for Mo Composite Catalysts

	R_{Mo-C}[a] (Å)	N_{Mo-C}[b]	R_{Mo-Mo}[a] (Å)	N_{Mo-Mo}[b]	R-factor[c]
Mo_2C	2.11(1)	2.9(3)	2.97(1)	8.9(3)	0.003
Mo_2C/CNT−GR	2.10(1)	2.7(3)	2.98(1)	8.3(3)	0.004
Mo_2N	2.10(1)	2.7(1)	2.88(1)	4.6(2)	0.006
Mo_2N/CNT−GR	2.10(1)	2.8(1)	2.88(2)	4.6(2)	0.007
MoS_2	2.40(1)	3.4(2)	3.16(1)	2.4(3)	0.018
MoS_2/CNT−GR	2.40(1)	3.1(2)	3.15(1)	1.9(3)	0.022

[a] Bond distance. [b] Coordination number. [c] A sum-of-square measure of the fractional misfit. The number in parentheses denotes an uncertainty of the calculated parameters at the last digit place.

TABLE 2. Electric Properties of the Synthesized Catalysts

catalyst	sheet resistance[a] [Ω □$^{-1}$]	conductivity[a] [S m^{-1}]	Tafel slope[b] [mV dec^{-1}]	J_0[b] [mA cm^{-2}]	R_{ct}[c] [Ω]	capacitance[c] [μF]
Mo_2C/CNT−GR	1.29 (±0.14)	3.10×10^3	58	6.20×10^{-2}	4.28	4912
Mo_2N/CNT−GR	2.17 (±0.29)	1.84×10^3	72	3.94×10^{-2}	21.61	7958
MoS_2/CNT−GR	37.73 (±3.48)	1.06×10^2	100	2.91×10^{-2}	99.0	2535

[a] From 4-point probe method. [b] From Tafel plots in Figure 3b. [c] Extracted from fitting electrochemical impedance spectra measured at $\eta = 200$ mV to an equivalent circuit.

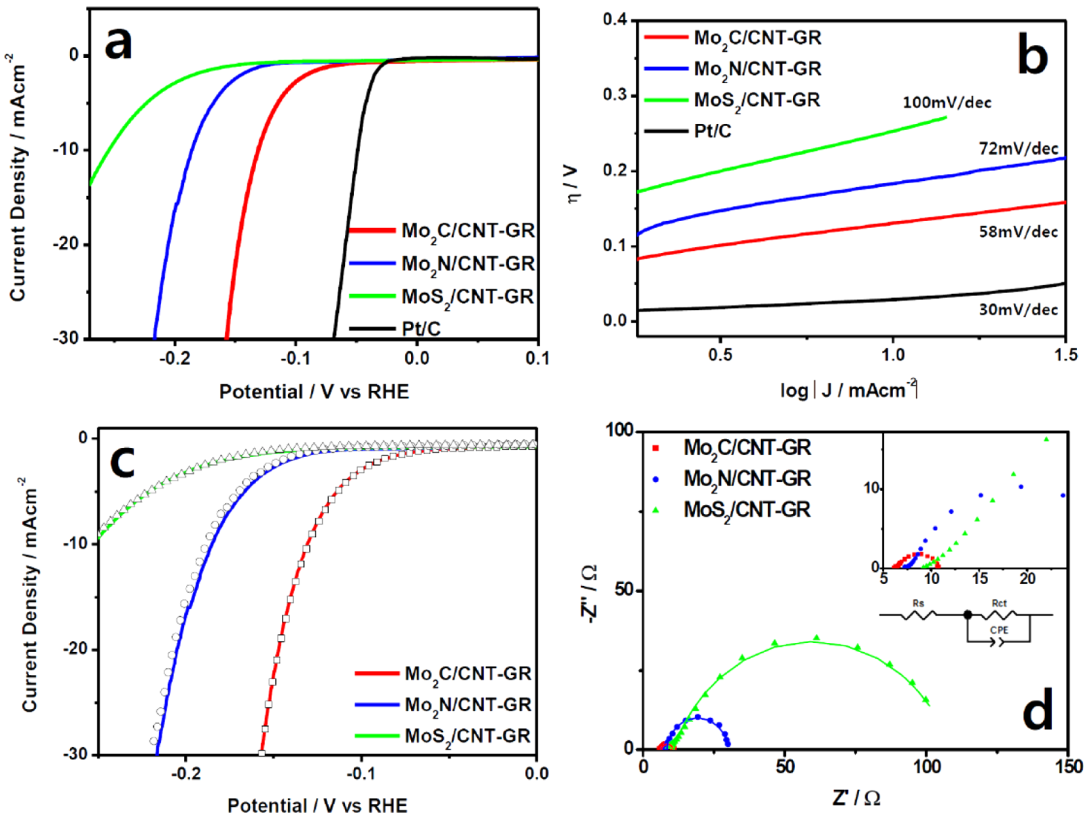

Figure 3. Electrochemical characterization of the prepared catalysts. (a) polarization curves, (b) Tafel plots, (c) stability measurements (empty rectangles, circles, and triangles depict the current densities of each catalyst after 1000 repeated potential cyclings), and (d) Nyquist plots with an equivalent curcuit. Inset of (d) denotes the magnified images of high frequency region.

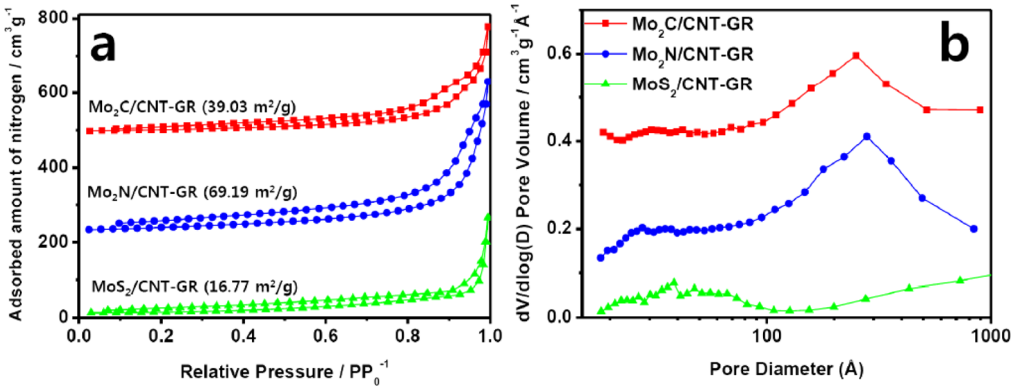

Figure 4. (a) N_2-sorption isotherms and (b) pore size distribution plots of the synthesized catalysts.

the loaded Mo-compounds. The CNT−GR support substantially increased the conductivity of the synthesized catalysts, provided high surface area to contact with electrolyte, and dispersed the Mo-compound nanoparticles without aggregation. In case of MoS_2/CNT−GR, it exhibited fairly lower performance for HER than Mo_2C/CNT−GR or Mo_2N/CNT−GR. As discussed above, relatively high synthetic temperature for MoS_2 resulted in sintering of MoS_2 nanocrystals, which reduced the number of exposed active edge sites and lowered the activity of MoS_2/CNT−GR. Indeed, N_2-sorption measurements in Figure 4a revealed that MoS_2/CNT−GR exhibited the lowest BET surface area of 16.8 m^2/g. Furthermore, unlike Mo_2C/CNT−GR and Mo_2N/CNT−GR, large pores above 10 nm were not generated effectively (Figure 4b).

We have further investigated their activities by determining exchange current densities (J_0), which represent the intrinsic activities of Mo-compounds for HER. As shown in Table 2, Mo_2C/CNT−GR exhibited the highest J_0 value indicating its high intrinsic activity for HER. However, further development is required for Mo_2C catalysts because its J_0 value is still 1 order of magnitude lower than that of Pt/C

(5.41×10^{-1} mA cm^{-2}). In spite of the fundamental significance of Tafel slopes and J_0 values, their measurement from Tafel plot is rather arbitrary because of the choice of the regions on the Tafel plots or different methods of *iR*-correction. Thus, comparing the required overpotentials for driving a current of 10 mA cm^{-2} (η_{10}) is more practical as conducted by Chen *et al.*[22] In addition, a solar light-coupled HER apparatus usually runs at 10−20 mA cm^{-2} under the standard condition (1 sun, AM 1.5)[36] indicating that 10 mA cm^{-2} is meaningful as the point of reference. The η_{10} values were determined to be 130, 186, and 255 mV for Mo_2C/CNT−GR, Mo_2N/CNT−GR, and MoS_2/CNT−GR, respectively. Furthermore, mass activity at 150 mV of Mo_2C/CNT−GR (33.5 mA mg^{-1}) was 10 to 20 times higher than those of Mo_2N/CNT−GR (3.5) and MoS_2/CNT−GR (1.5). As shown in Table S2 (SI), the performance of our Mo_2C/CNT−GR is one of the best among many recently reported Mo-based electrocatalysts with a low η_{10} values and high mass activity at 150 mV.[14,15,17,21−23,37] For broader comparison, representative nonprecious metal catalysts are also included in Table S1 (SI) such as tungsten carbide,[10] iron tungsten carbonitride,[38] and nickel phosphide.[39]

Stability in acid media is an important issue to be a practical catalyst for HER in PEM electrolyzer. Our Mo_2C/CNT−GR exhibited very good electrochemical stability showing negligible activity loss after a thousand potential-cycling tests between −0.3 and 0.2 V as shown in Figure 3c. Mo_2N/CNT−GR showed a slight activity loss after stability test, but the synthesized Mo-compounds/CNT−GR generally exhibited good stability. Such a good stability and activity of our Mo_2C/CNT−GR electocatalyst demonstrate the effectiveness of our synthetic technique to manufacture the practical Mo-based eletrocatalysts for HER.

Electrochemical impedance spectroscopy (EIS) measurements were conducted for further characterization of the synthesized catalysts. Figure 3d displays the obtained Nyquist plots, and the magnified Nyquist plots in low frequency region are presented for clarity (upper inset of Figure 3d). The data were fitted to an equivalent circuit shown in the inset of Figure 3d, and the resultant fitting parameters are summarized in Table 2. A semicircle in the Nyquist plot represents the charge transfer process at the interface between electrocatalyst and electrolyte, which is consisted of charge transfer resistance (R_{ct}) and corresponding capacitance. In general, R_{ct} value varies inversely to the electrocatalytic activity. The obtained R_{ct} value of Mo_2C/CNT−GR (4.28 Ω) is much lower than those of Mo_2N/CNT−GR (21.61 Ω) and MoS_2/CNT−GR (99.0 Ω). Thus, such a low R_{ct} value of Mo_2C/CNT−GR indicates that its high electrocatalytic activity for HER could be ascribed to the highly conductive CNT−GR hybrid by improving the charge transfer characteristics of Mo_2C. MoS_2/CNT−GR exhibited a very high R_{ct} value, which would limit its HER activity critically by increasing the internal resistance. Hence, we could point out that the low activity of MoS_2/CNT−GR is attributed to its slow electron transfer, existence of inactive MoO_3 layer, low conductivity, and reduced number of exposed active sites. The capacitance is proportional to the contact area between the catalysts and electrolyte. Mo_2C/CNT−GR exhibits a higher capacitance value (4912 μF) compared to MoS_2/CNT−GR (2535 μF), but lower than those of Mo_2N/CNT−GR (7958 μF), which is consistent with the BET surface areas in Figure 4a. In electrocatalysis, high contact area is favorable for high activity. However, our Mo_2C/CNT−GR showed higher activity for HER than Mo_2N/CNT−GR in spite of lower contact area, suggesting that the intrinsic activity of Mo_2C is much higher than that of Mo_2N, and thus more than compensates for its lower contact area. The capacitance value of Mo_2C/CNT−GR was 1.6 times lower than that of Mo_2N/CNT−GR, but its R_{ct} value was 5 times lower. Furthermore, as discussed in XAFS results, Mo atoms in Mo_2C/CNT−GR is more electron deficient than Mo in Mo_2N/CNT−GR, and thus have lower hydrogen binding energy.

To demonstrate the effectiveness of CNT−GR hybrid support, Mo_2C nanocrystals are synthesized on several nanocarbon supports including CNT, GR, and carbon black (Vulcan XC72R). Their XRD patterns are identical with that of Mo_2C/CNT−GR in Figure S6a (SI), suggesting our synthetic method could be applied broadly to various carbon support materials. Figure S6b,c (SI) shows the TEM images of Mo_2C/CNT, Mo_2C/GR, and Mo_2C/C. The mean particle size of loaded Mo_2C nanocrystals is *ca.* 10 nm, which is consistent with the particle size of Mo_2C in Mo_2C/CNT−GR observed by XRD and TEM. Hence, we confirm that similar Mo_2C nanocrystals are properly synthesized on CNT, GR, and carbon black supports.

Raman spectra were collected to confirm reduced graphene in the prepared samples. In Figure S7 (SI), the intensity ratios between D peak and G peak (I_D/I_G ratios) were 0.86 for GO and 1.04 for Mo_2C/CNT−GR indicating the formation of GR from GO reduction. The increased I_D/I_G ratio relative to GO is commonly accepted indication of graphene formation.[40−42] However, the similar I_D/I_G ratio between CNT (1.03) and Mo_2C/CNT−GR (1.04) renders the existence of GR unclear. To exclude the interference of CNT, the Raman spectrum of Mo_2C/GR was measured, and its I_D/I_G ratio (1.02) clearly demonstrated the formation of GR from GO. These results lead us to conclude that GO was effectively reduced to GR in Mo_2C/CNT−GR.

Figure 5a exhibits the polarization curves for HER of the prepared Mo_2C/CNT, Mo_2C/GR, and Mo_2C/C samples with the Mo_2C/CNT−GR catalyst. In the whole potential range, Mo_2C/CNT−GR showed the superior current density compared to the other Mo_2C on different supports. The onset overpotential

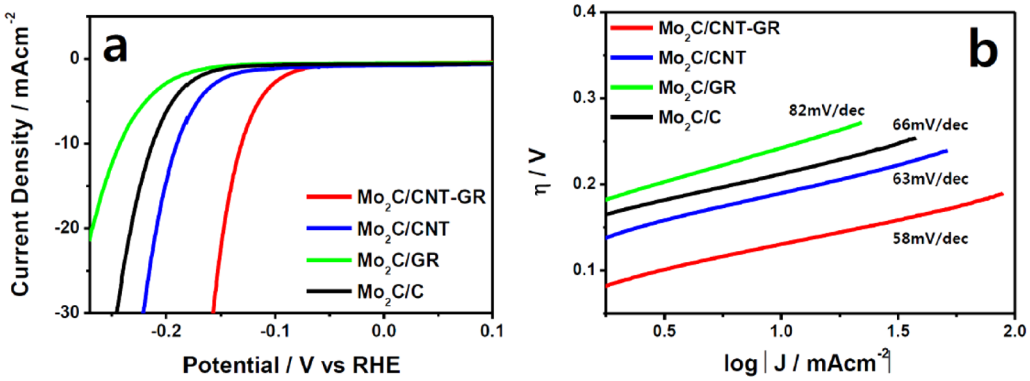

Figure 5. Electrochemical characterization of the prepared Mo_2C nanocrystals supported on the various carbon supports: (a) polarization curves, (b) Tafel plots.

of Mo_2C/CNT−GR (62 mV) was lower than those of Mo_2C/CNT (120 mV), Mo_2C/GR (150 mV), and Mo_2C/C (135 mV). Furthermore, the η_{10} values of Mo_2C/CNT (190 mV), Mo_2C/GR (242 mV), and Mo_2C/C (212 mV) were much higher than that of Mo_2C/CNT−GR (130 mV). In Figure 5b, the Tafel slope of Mo_2C/CNT−GR was smaller than the other Mo_2C catalysts. These results demonstrate the effectiveness of CNT−GR hybrid as a support material for Mo_2C nanocrystals. As discussed in our previous reports,[8,13] the excellent conductivity with much less bundling of CNT and stacking of GR and presence of the large pores due to the formation of three-dimensional structure between CNT and GR seem responsible for higher HER performance of Mo_2C/CNT−GR than Mo_2C on other carbon supports.

CONCLUSIONS

In summary, Mo_2C, Mo_2N, and MoS_2 nanocrystals on CNT−GR composites were synthesized by a modified urea-glass route. Through a simple modification by varying the amount of urea or replacement of urea with thiourea, it was possible to control the final phase of the products. The physicochemical characterizations including XRD and TEM investigations verified that the high purity Mo_2C, Mo_2N, and MoS_2 nanocrystals were well anchored on CNT−GR hybrid revealing the effectiveness of our synthetic method. The electrochemical characterizations revealed the excellent activity of our Mo_2C/CNT−GR for HER compared to Mo_2N/CNT−GR and MoS_2/CNT−GR. The obtained Tafel slope, J_0, and η_{10} values of Mo_2C/CNT−GR were 58 mV dec^{-1}, 6.20 × 10^{-2} mA cm^{-2}, and 130 mV, respectively, which represent one of the best performances among recently reported Mo-based electrocatalysts. The Mo atoms in Mo_2C have more positive charge, which induces the downshift of d-band center and decrease in hydrogen binding energy. Also, the CNT−GR hybrid as a support plays crucial roles to enhance the activity of Mo-compounds by alleviating the aggregation between the Mo-compounds, providing a large area to contact with electrolyte, and facilitating the electron transfer. Thus, the Mo_2C/CNT−GR could be a promising electrocatalyst for HER because of its good activity, stability, and low price.

METHODS

Catalyst Fabrication. Mo_2C, Mo_2N, and MoS_2 nanocrystals loaded on CNT−GR support were synthesized by modified urea-glass route described elsewhere.[8,13] GO was prepared by Hummer's method,[43] and CNT was purchased from Hanwha Nanotech (multiwalled CNT, CM-95). GO and CNT was dispersed in 15 mL of ethanol with a 1:1 weight ratio. 1.0 g of $MoCl_5$ was dissolved in 2.5 mL of ethanol, which was moved to the CNT−GO containing solution. For Mo_2C synthesis, proper amount of urea with molar ratio of urea/Mo (R) = 8, was added to the solution. Here, by decreasing the amount of urea (R = 1) or replacing urea with thiourea (R = 2), Mo_2N or MoS_2 catalysts could be obtained, respectively. After vigorous stirring with urea for 1 h, the resulting solution was dried in a 100 °C oven to remove the excess ethanol, and calcined at 750 °C for 3 h under N_2 flow. Through the synthesis, the nominal content of each Mo-compound was fixed at *ca.* 75 wt %, and the resultant experimental contents of Mo-compounds were determined to be *ca.* 65 wt % for Mo_2C/CNT−GR and MoS_2/CNT−GR, and 67 wt % for Mo_2N/CNT−GR by ICP measurements (Table S2 (SI)).

Catalyst Characterization. Crystalline structures of the prepared catalysts were analyzed by X-ray diffraction (XRD) with a PANalytical pw 3040/60 X'pert diffractometer. Structural information was revealed by a high resolution transmission electron microscope (TEM, JEOL, JEM-2100F). Surface areas and pore size distribution of the catalysts were characterized by N_2-sorption isotherms measured at 77 K (Mirae scientific instruments, Nanoporosity-XQ). Conductivity of the catalysts was measured by the four-point probe method (Keithley 2400) using a pelletized sample (thin disk type) without any additives. The thickness of the pelletized samples was 250 μm. X-ray absorption fine structure (XAFS) measurements were conducted to investigate the local structures of the Mo composite catalysts on 7D beamline of the Pohang Accelerator Laboratory (PLS-II, 3.0 GeV), Korea. The incident beam was monochromatized using a Si (111) double crystal monochromator. At room temperature, the spectra were taken for the K-edge of Mo (E_0 = 2.0 × 10^4 eV) in a transmission mode with separate N_2-filled IC Spec ionization chambers for incident and transmitted beams. For each sample, the reference spectra of Mo foil was taken simultaneously so that the energy in the spectrum of sample could be calibrated with the respect to the K-edge energy of Mo metal. The obtained data were analyzed with ATHENA and ARTEMIS in the IFEFIT suite of software programs.[44] FEFF 9 code was used to

synthesize theoretical EXAFS spectra for nonlinear square fittings of samples.[45] Hydrogen temperature-programmed desorption (H_2-TPD) measurements were carried out to identify the hydrogen binding energy on the synthesized catalysts using a chemisorption analyzer (Micromeritics, autochem II). The samples (50 mg) were exposed to a flow of 10% H_2 diluted in Ar gas for 1 h followed by heating to 800 °C with a ramping rate of 10 °C/min.

Electrochemical Tests. Linear sweep voltammetry (LSV) and durability tests were conducted in a three electrode cell with N_2-saturated aqueous solution of 0.5 M H_2SO_4 using a potentiostat (Ivium technologies) equipped with a rotating disk electrode setup (RDE, PAR Model 636 RDE). The Ag/AgCl electrode and a Pt wire were used as reference and counter electrodes, respectively. All the potentials were referred to the reversible hydrogen electrode (RHE) without specification. The working electrodes were prepared by dispersing 20 mg of catalyst in 2.0 mL of deionized water and 40 μL of 5% Nafion solution and pipetting out 20 μL of slurry onto a glassy carbon electrode (0.65−0.67 mg cm^{-2} loading of Mo-compounds). 9 μL of Nafion solution was added on top to fix the electrocatalyst. The LSV tests were performed at a scan rate of 5 mV s^{-1} with 900 rpm, which were measured after 20 cycles of cyclic voltammetry (CV) tests in the range of 0.4 to −0.3 V to stabilize the current. The durability tests were carried out by repeating the potential scan from 0.4 to −0.3 V with 1000 cycles. In the identical cell setup, electrochemical impedance spectroscopy (EIS) was carried out. The frequency range was from 100 kHz to 1 mHz with a modulation amplitude of 10 mV at −0.2 V bias voltage. The EIS spectra were fitted by the Z-view software.

Conflict of Interest: The authors declare no competing financial interest.

Acknowledgment. This work was supported by Brain Korea Plus Program of Ministry of Education, and Basic Science Research Program (No. 2012-017247) and Korean Center for Artificial Photosynthesis (NRF-2011-C1AAA0001-2011-0030278) funded by the Ministry of Science, ICT and Future Planning of Republic of Korea.

Supporting Information Available: TEM, XANES, H_2-TPD, Raman and LSV results of the samples. This material is available free of charge *via* the Internet at http://pubs.acs.org.

REFERENCES AND NOTES

1. Laursen, A. B.; Kegnaes, S.; Dahl, S.; Chorkendorff, I. Molybdenum Sulfides-Efficient and Viable Materials for Electro- and Photoelectrocatalytic Hydrogen Evolution. *Energy Environ. Sci.* **2012**, *5*, 5577–5591.
2. Chen, W.-F.; Muckerman, J. T.; Fujita, E. Recent Developments in Transition Metal Carbides and Nitrides as Hydrogen Evolution Electrocatalysts. *Chem. Commun.* **2013**, *49*, 8896–8909.
3. Esposito, D. V.; Hunt, S. T.; Kimmel, Y. C.; Chen, J. G. A New Class of Electrocatalysts for Hydrogen Production from Water Electrolysis: Metal Monolayers Supported on Low-Cost Transition Metal Carbides. *J. Am. Chem. Soc.* **2012**, *134*, 3025–3033.
4. Esposito, D. V.; Hunt, S. T.; Stottlemyer, A. L.; Dobson, K. D.; McCandless, B. E.; Birkmire, R. W.; Chen, J. G. Low-Cost Hydrogen-Evolution Catalysts Based on Monolayer Platinum on Tungsten Monocarbide Substrates. *Angew. Chem., Int. Ed.* **2010**, *49*, 9859–9862.
5. Norskov, J. K.; Bligaard, T.; Logadottir, A.; Kitchin, J. R.; Chen, J. G.; Pandelov, S.; Stimming, U. Trends in the Exchange Current for Hydrogen Evolution. *J. Electrochem. Soc.* **2005**, *152*, J23–J26.
6. Furimsky, E. Metal Carbides and Nitrides as Potential Catalysts for Hydroprocessing. *Appl. Catal., A* **2003**, *240*, 1–28.
7. Chen, J. G. Carbide and Nitride Overlayers on Early Transition Metal Surfaces: Preparation, Characterization, and Reactivities. *Chem. Rev.* **1996**, *96*, 1477–1498.
8. Youn, D. H.; Bae, G.; Han, S.; Kim, J. Y.; Jang, J.-W.; Park, H.; Choi, S. H.; Lee, J. S. A Highly Efficient Transition Metal Nitride-based Electrocatalyst for Oxygen Reduction Reaction: TiN on a CNT-Graphene Hybrid Support. *J. Mater. Chem. A* **2013**, *1*, 8007–8015.
9. Ham, D.; Lee, J. Transition Metal Carbides and Nitrides as Electrode Materials for Low Temperature Fuel Cells. *Energies* **2009**, *2*, 873–899.
10. Garcia-Esparza, A. T.; Cha, D.; Ou, Y.; Kubota, J.; Domen, K.; Takanabe, K. Tungsten Carbide Nanoparticles as Efficient Cocatalysts for Photocatalytic Overall Water Splitting. *ChemSusChem* **2013**, *6*, 168–181.
11. Jang, J. S.; Ham, D. J.; Lakshminarasimhan, N.; Choi, W.; Lee, J. S. Role of Platinum-like Tungsten Carbide as Cocatalyst of CdS Photocatalyst for Hydrogen Production under Visible Light Irradiation. *Appl. Catal., A* **2008**, *346*, 149–154.
12. Youn, D. H.; Seol, M.; Kim, J. Y.; Jang, J.-W.; Choi, Y.; Yong, K.; Lee, J. S. TiN Nanoparticles on CNT−Graphene Hybrid Support as Noble-Metal-Free Counter Electrode for Quantum-Dot-Sensitized Solar Cells. *ChemSusChem* **2013**, *6*, 261–267.
13. Seol, M.; Youn, D. H.; Kim, J. Y.; Jang, J.-W.; Choi, M.; Lee, J. S.; Yong, K. Mo-Compound/CNT-Graphene Composites as Efficient Catalytic Electrodes for Quantum-Dot-Sensitized Solar Cells. *Adv. Energy Mater.* **2014**, *4*, 1300775.
14. Vrubel, H.; Hu, X. Molybdenum Boride and Carbide Catalyze Hydrogen Evolution in both Acidic and Basic Solutions. *Angew. Chem., Int. Ed.* **2012**, *51*, 12703–12706.
15. Chen, W.-F.; Sasaki, K.; Ma, C.; Frenkel, A. I.; Marinkovic, N.; Muckerman, J. T.; Zhu, Y.; Adzic, R. R. Hydrogen-Evolution Catalysts Based on Non-Noble Metal Nickel−Molybdenum Nitride Nanosheets. *Angew. Chem., Int. Ed.* **2012**, *51*, 6131–6135.
16. Hinnemann, B.; Moses, P. G.; Bonde, J.; Jørgensen, K. P.; Nielsen, J. H.; Horch, S.; Chorkendorff, I.; Nørskov, J. K. Biomimetic Hydrogen Evolution: MoS_2 Nanoparticles as Catalyst for Hydrogen Evolution. *J. Am. Chem. Soc.* **2005**, *127*, 5308–5309.
17. Li, Y.; Wang, H.; Xie, L.; Liang, Y.; Hong, G.; Dai, H. MoS2 Nanoparticles Grown on Graphene: An Advanced Catalyst for the Hydrogen Evolution Reaction. *J. Am. Chem. Soc.* **2011**, *133*, 7296–7299.
18. Kibsgaard, J.; Chen, Z.; Reinecke, B. N.; Jaramillo, T. F. Engineering the Surface Structure of MoS_2 to Preferentially Expose Active Edge Sites for Electrocatalysis. *Nat. Mater.* **2012**, *11*, 963–969.
19. Liao, L.; Zhu, J.; Bian, X.; Zhu, L.; Scanlon, M. D.; Girault, H. H.; Liu, B. MoS_2 Formed on Mesoporous Graphene as a Highly Active Catalyst for Hydrogen Evolution. *Adv. Funct. Mater.* **2013**, *23*, 5326–5333.
20. Chang, Y.-H.; Lin, C.-T.; Chen, T.-Y.; Hsu, C.-L.; Lee, Y.-H.; Zhang, W.; Wei, K.-H.; Li, L.-J. Highly Efficient Electrocatalytic Hydrogen Production by MoS_x Grown on Graphene-Protected 3D Ni Foams. *Adv. Mater.* **2013**, *25*, 756–760.
21. Chen, W. F.; Wang, C. H.; Sasaki, K.; Marinkovic, N.; Xu, W.; Muckerman, J. T.; Zhu, Y.; Adzic, R. R. Highly Active and Durable Nanostructured Molybdenum Carbide Electrocatalysts for Hydrogen Production. *Energy Environ. Sci.* **2013**, *6*, 943–951.
22. Chen, W.-F.; Iyer, S.; Iyer, S.; Sasaki, K.; Wang, C.-H.; Zhu, Y.; Muckerman, J. T.; Fujita, E. Biomass-Derived Electrocatalytic Composites for Hydrogen Evolution. *Energy Environ. Sci.* **2013**, *6*, 1818–1826.
23. Liao, L.; Wang, S.; Xiao, J.; Bian, X.; Zhang, Y.; Scanlon, M. D.; Hu, X.; Tang, Y.; Liu, B.; Girault, H. H.; Nanoporous, A. Molybdenum Carbide Nanowire as an Electrocatalyst for Hydrogen Evolution Reaction. *Energy Environ. Sci.* **2014**, *7*, 387–392.
24. Giordano, C.; Erpen, C.; Yao, W.; Milke, B.; Antonietti, M. Metal Nitride and Metal Carbide Nanoparticles by a Soft Urea Pathway. *Chem. Mater.* **2009**, *21*, 5136–5144.
25. Pei, S.; Cheng, H.-M. The Reduction of Graphene Oxide. *Carbon* **2012**, *50*, 3210–3228.
26. Zhang, D.; Yan, T.; Shi, L.; Peng, Z.; Wen, X.; Zhang, J. Enhanced Capacitive Deionization Performance of

Graphene/Carbon Nanotube Composites. *J. Mater. Chem.* **2012**, *22*, 14696–14704.
27. Koroteev, V. O.; Bulusheva, L. G.; Asanov, I. P.; Shlyakhova, E. V.; Vyalikh, D. V.; Okotrub, A. V. Charge Transfer in the MoS_2/Carbon Nanotube Composite. *J. Phys. Chem. C* **2011**, *115*, 21199–21204.
28. Xiang, Q.; Yu, J.; Jaroniec, M. Synergetic Effect of MoS_2 and Graphene as Cocatalysts for Enhanced Photocatalytic H_2 Production Activity of TiO_2 Nanoparticles. *J. Am. Chem. Soc.* **2012**, *134*, 6575–6578.
29. Liu, P.; Rodriguez, J. A.; Muckerman, J. T. Desulfurization of SO_2 and Thiophene on Surfaces and Nanoparticles of Molybdenum Carbide: Unexpected Ligand and Steric Effects. *J. Phys. Chem. B* **2004**, *108*, 15662–15670.
30. Shi, C.; Zhang, A.; Li, X.; Zhang, S.; Zhu, A.; Ma, Y.; Au, C. Ni-modified Mo_2C Catalysts for Methane Dry Reforming. *Appl. Catal., A* **2012**, *431*−*432*, 164–170.
31. Wei, Z. B. Z.; Grange, P.; Delmon, B. XPS and XRD Studies of Fresh and Sulfided Mo_2N. *Appl. Surf. Sci.* **1998**, *135*, 107–114.
32. Vo, D.-V. N.; Adesina, A. A. A Potassium-Promoted Mo Carbide Catalyst System for Hydrocarbon Synthesis. *Catal. Sci. Technol.* **2012**, *2*, 2066–2076.
33. Li, X.; Chen, Y.; Zhang, Y.; Ji, C.; Xin, Q. Temperature-Programmed Desorption and Adsorption of Hydrogen on Mo_2N. *React. Kinet. Catal. Lett.* **1996**, *58*, 391–396.
34. Bao, J.; Fu, Y.-L.; Bian, G.-Z. Sol−gel Preparation of K−Co−Mo Catalyst and its Application in Mixed Alcohol Synthesis from CO Hydrogenation. *Catal. Lett.* **2008**, *121*, 151–157.
35. McGarvey, G. B.; Kasztelan, S. An Investigation of the Reduction Behavior of MoS_2/Al_2O_3 and the Subsequent Detection of Hydrogen on the Surface. *J. Catal.* **1994**, *148*, 149–156.
36. Walter, M. G.; Warren, E. L.; McKone, J. R.; Boettcher, S. W.; Mi, Q.; Santori, E. A.; Lewis, N. S. Solar Water Splitting Cells. *Chem. Rev.* **2010**, *110*, 6446–6473.
37. Tran, P. D.; Nguyen, M.; Pramana, S. S.; Bhattacharjee, A.; Chiam, S. Y.; Fize, J.; Field, M. J.; Artero, V.; Wong, L. H.; Loo, J.; Barber, J. Copper Molybdenum Sulfide: a New Efficient Electrocatalyst for Hydrogen Production from Water. *Energy Environ. Sci.* **2012**, *5*, 8912–8916.
38. Zhao, Y.; Kamiya, K.; Hashimoto, K.; Nakanishi, S. Hydrogen Evolution by Tungsten Carbonitride Nanoelectrocatalysts Synthesized by the Formation of a Tungsten Acid/Polymer Hybrid *In Situ*. *Angew. Chem., Int. Ed.* **2013**, *125*, 13883–13886.
39. Popczun, E. J.; McKone, J. R.; Read, C. G.; Biacchi, A. J.; Wiltrout, A. M.; Lewis, N. S.; Schaak, R. E. Nanostructured Nickel Phosphide as an Electrocatalyst for the Hydrogen Evolution Reaction. *J. Am. Chem. Soc.* **2013**, *135*, 9267–9270.
40. Stankovich, S.; Dikin, D. A.; Piner, R. D.; Kohlhaas, K. A.; Kleinhammes, A.; Jia, Y.; Wu, Y.; Nguyen, S. T.; Ruoff, R. S. Synthesis of Graphene-Based Nanosheets *via* Chemical Reduction of Exfoliated Graphite Oxide. *Carbon* **2007**, *45*, 1558–1565.
41. Cui, P.; Lee, J.; Hwang, E.; Lee, H. One-Pot Reduction of Graphene Oxide at Subzero Temperatures. *Chem. Commun.* **2011**, *47*, 12370–12372.
42. Choi, E.-Y.; Han, T. H.; Hong, J.; Kim, J. E.; Lee, S. H.; Kim, H. W.; Kim, S. O. Noncovalent Functionalization of Graphene with End-functional Polymers. *J. Mater. Chem.* **2010**, *20*, 1907–1912.
43. Hummers, W. S.; Offeman, R. E. Preparation of Graphitic Oxide. *J. Am. Chem. Soc.* **1958**, *80*, 1339–1339.
44. Ravel, B.; Newville, M. ATHENA, ARTEMIS, HEPHAESTUS: Data Analysis for X-ray Absorption Spectroscopy using IFEFFIT. *J. Synchrotron Radiat.* **2005**, *12*, 537–541.
45. Rehr, J. J.; Kas, J. J.; Vila, F. D.; Prange, M. P.; Jorissen, K. Parameter-free Calculations of X-ray Spectra with FEFF9. *Phys. Chem. Chem. Phys.* **2010**, *12*, 5503–5513.